KSCE Journal of Civil Engineering (2022) 26(8):3486-3503
DOI 10.1007/s12205-022-1188-9

pISSN 1226-7988, eISSN 1976-3808
www.springer.com/12205

Structural Engineering

Performance-Based Seismic Design of Corrugated Steel Plate Shear Walls

Qiuhong Zhao[a,b], **Jing Qiu**[a], **Yu Zhao**[c], **and Cheng Yu**[d]

[a]*School of Civil Engineering, Tianjin University, Tianjin 300350, China*
[b]*Key Laboratory of Coast Civil Structure and Safety of Ministry of Education, Tianjin University, Tianjin 300072, China*
[c]*China Railway Design Corporation Co., Ltd., Tianjin 300308, China*
[d]*Dept. of Mechanical Engineering, University of North Texas, Denton, TX 76207, USA*

ARTICLE HISTORY

Received 1 July 2021
Revised 28 October 2021
Accepted 27 February 2022
Published Online 9 June 2022

KEYWORDS

Corrugated steel plate shear walls
Performance-based seismic design
Target drift
Ideal yield mechanism
Uniform inelastic deformation
Fragility curves

ABSTRACT

Corrugated steel plate shear walls (CoSPSWs) consist of corrugated steel wall plates and a steel boundary frame, which could be adopted as seismic-resistant systems for high-rise buildings. In this study, a performance-based seismic design (PBSD) method was proposed for CoSPSWs, in which an ideal yield mechanism and target drifts were selected as performance objectives to evaluate and control the inelastic behavior of the system. Two 10-story CoSPSW structures were then designed with the PBSD method and the traditional method respectively, and static pushover analyses as well as nonlinear dynamic time-history analyses were conducted on both structures. It turned out that the CoSPSW structure designed with the PBSD method presented the ideal yield mechanism, all inter-story drifts were well below the target drift of 2.5%, and the drifts distributed more smoothly under rare earthquakes. Structural and nonstructural fragility curves of both CoSPSW structures were obtained through probabilistic seismic demand analysis using Incremental Dynamic Analyses. The results showed that for the structural repair states of RS1 to RS5, the 25th percentile PGA values of the fragility curves of the CoSPSW structure designed with the PBSD method were 220%, 98%, 84%, 51% and 13% higher than the CoSPSW structure designed with the traditional method, respectively. For the nonstructural damage states of Slight to Complete, the 25th percentile PGA values of the fragility curves of the CoSPSW structure designed with the PBSD method were 145%, 98%, 36%, and 7% higher than the CoSPSW structure designed with the traditional method, respectively. Therefore, CoSPSW structure designed with the PBSD method had lower seismic vulnerability as well as probability of nonstructural damage.

1. Introduction

Corrugated steel plate shear wall (CoSPSW) is a new type of steel plate shear wall in which corrugated wall plates are embedded inside a steel boundary frame, instead of flat wall plates in conventional steel plate shear walls (SPSWs), as shown in Fig. 1 below. CoSPSWs have high lateral stiffness, good ductility and high energy dissipation capacity, which makes them good seismic-resistant systems for high-rise buildings (Emami et al., 2013; Dou et al., 2016; Zhao et al., 2017; Qiu et al., 2018). Compared to flat wall plates, corrugated wall plates have significantly higher out-of-plane rigidity and buckling capacity, therefore buckling of the wall plates could be avoided under the serviceability limit state, which makes it easier to satisfy the current Chinese design specification (JGJ99-2015, 2016). Moreover, the “Accordion Effects” resulting from the corrugation could help to minimize the gravity loads transferred to the wall plate during construction, and facilitate a synchronized installation with the rest of the story, which significantly enhances the construction speed especially for high-rise buildings. Unlike conventional flat wall plates that relies on the tension-field action to resist the lateral load, corrugated wall plates rely mostly on in-plane shear yielding (Qiu et al., 2018), and thus pinching of the hysteric curves from buckling could be obviously improved and energy dissipation could be increased accordingly (Kalali et al., 2015; Zhao et al., 2017).

Research on CoSPSWs has just started in the past two decades. Berman and Bruneau (2005), Stojadinovic and Tipping (2008), Emami et al. (2013), Hosseinzadeh et al. (2017), Ding et al. (2017),

CORRESPONDENCE Qiuhong Zhao ✉ qzhao@tju.edu.cn School of Civil Engineering, Tianjin University, Tianjin 300350, China; Key Laboratory of Coast Civil Structure and Safety of Ministry of Education, Tianjin University, Tianjin 300072, China

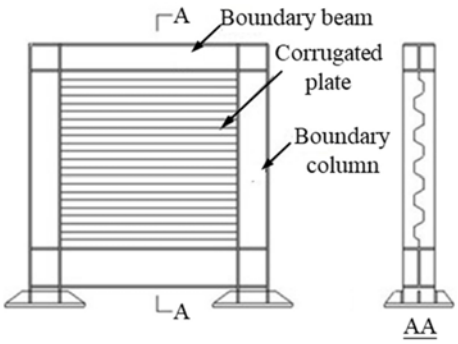

Fig. 1. Typical CoSPSWs

Cao and Huang (2018), and Qiu et al. (2018) have conducted cyclic tests on corrugated steel shear walls with different number of stories, aspect ratios, corrugation configurations including the corrugation angle, subpanel width, corrugation depth, etc. Theoretical and numerical analyses have been conducted on the cyclic and lateral behavior of corrugated steel plate shear walls with different corrugation layout directions, corrugation shapes, wall plate thicknesses, boundary frame members, corrugation configurations including the corrugation angle, corrugation depth, corrugation length, subpanel width, etc. by Emami and Mofid (2014), Edalati et al. (2014), Kalali et al. (2015), Zhao et al. (2017), Tong and Guo (2018), Dou et al. (2016) and Farzampour et al. (2018a). Furthermore, extended research has been conducted on corrugated steel shear walls with perforations or openings (Farzampour and Yekrangnia, 2014; Farzampour and Laman, 2015; Bahrebar et al., 2016; Bahrebar et al., 2020), reduced beam section (Masoud and Mahna, 2018; Farzampour et al., 2018b), semi-rigid boundary frame (Fang et al., 2020), low-yield point steel wall panel (Shariati et al., 2019), as well as application of corrugated steel shear walls in modular structural design (Yu and Chen, 2018). Latest research has been conducted to investigate the effects of semi-rigid wall-frame connections on the lateral behavior of SPSWs with flat wall plates (Paslar et al., 2020a; Paslar et al., 2020b), which could be considered for corrugated steel plate shear walls in the future.

In current design specifications, such as the AISC Seismic Provisions (ANSI/AISC 341-16, 2016), Canadian design standard (CAN/CSA S16-2014, 2014) and Chinese design specification (JGJ99-2015, 2016), the capacity design procedure is adopted for seismic design of flat steel plate shear walls, in which wall thickness is firstly determined for each story from elastic lateral force distribution, then the boundary columns and beams are designed to resist the external loads as well as yielding forces of the diagonal tension field in the wall plate (Sabelli and Bruneau, 2007; Qu and Bruneau, 2010). For CoSPSWs, modifications have been made on the yielding forces of the wall plate on the boundary columns and beams, which were considered a combination of elastic shear buckling and tension field action (Zhao and Li, 2016; Qiu et al., 2018; Farzampour et al., 2018b).

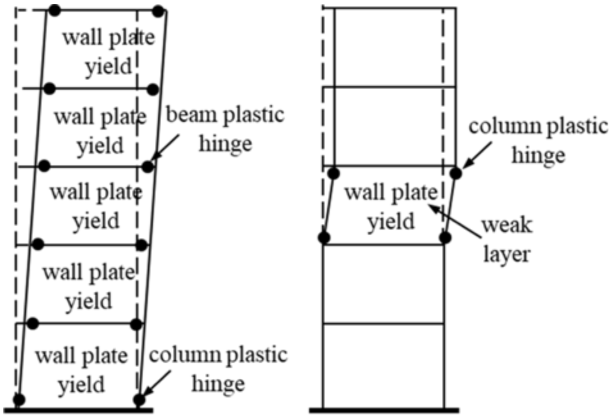

(a) (b)

Fig. 2. Yield Mechanism of Steel Plate Shear Walls: (a) Ideal Yield Mechanism, (b) Yield Mechanism with Weak Layer

However, the capacity design procedure is based on an ideal yield mechanism shown in Fig. 2(a) (Berman and Bruneau, 2003), which involves yielding of the wall plates and formation of plastic hinges at boundary beam ends in all stories simultaneously. Berman (2011) conducted nonlinear time-history analyses on code-designed SPSWs, and pointed out that for taller SPSWs, the capacity design procedures might be quite conservative, since it is unlikely that of the web plates and boundary beam ends would yield in all stories simultaneously. Moreover, although the failure mode of a given story could be controlled such that the wall plate yields before the boundary frame members, seismic response of the building would still be unpredictable, and might deviate significantly from the original design assumptions, as the structure enters the inelastic stage. For example, the distribution mode of story shear force in the design specifications is generally based on building behavior in the elastic stage, which could be quite different from the actual distribution mode of story shear force in the inelastic stage. Therefore, lateral strength of the designed SPSW might not match the story shear distribution precisely after the building enters the inelastic stage, which could lead to a concentration of story drift, i.e., forming of a weak layer shown in Fig. 2(b), and cause severe damage or even collapse (Chao et al., 2007; Berman, 2011).

As a result, the performance-based seismic design (PBSD) method has started to be applied to SPSWs, which could give a better understanding of the inherent structural behavior during strong earthquake ground motions as a promising and effective seismic design method (SEAOC, 1995; Leelataviwat, 1998; Soonsik, 2002). Compared to traditional seismic design methods including the capacity design procedure that only considers the inelastic structural behavior indirectly through modification factors, the PBSD method directly uses the inelastic response parameters such as inelastic lateral displacement, ductility ratio, hysteretic energy dissipation etc. to quantify the seismic damages, so that the structural behavior could be evaluated and predicted in a more accurate way. Furthermore, the traditional design method only focuses on the ratio between the demand and capacity at member level, so the overall structural performance might be strongly affected by the weakest or least-ductile member, whereas the PBSD method pays more attention to the global structural response (Hamburger at al., 2004). Therefore, structural performance from the PBSD method would be more desirable and predictable under design level earthquakes, especially under strong earthquakes.

PBSD method has been proposed for conventional flat SPSWs with pinned beam-to-column connections and the design base shear formula was modified to account for the pinched hysteretic behavior, with the yield mechanism and maximum lateral drift as two performance targets. Four-story SPSWs were designed using the PBSD method, and the intended target drift and yield mechanisms were successfully achieved (Bayat, 2010). PBSD method has also been proposed for flat SPSWs with rigid beam-to-column connections and the design base shear formula was modified to consider the P-delta effects by Kharmale and Ghosh (2013), with the yield mechanism and ductility ratio as two performance targets. Four-story and eight-story SPSWs were designed using the PBSD method, and the intended target ductility ratio and yield mechanisms were successfully achieved. Studies have also been carried out on different design parameters for performance-based seismic design of flat and corrugated steel plate shear walls, including the damage/repair states and associated drift levels of flat steel plate shear walls (Baldvins et al., 2012; Zhang and Zirakian, 2015), inelastic lateral force distribution mode of flat steel plate shear walls (Sun et al., 2013), and the fundamental period formulas of flat and corrugated steel plate shear walls (Topkaya and Kurban, 2009; Bhowmick et al., 2011; Liu et al., 2013; Zhao et al., 2020).

In this paper, a PBSD method is proposed for CoSPSWs, which have very different lateral load-carrying mechanism, plate-frame interaction and hysteretic behavior from convention flat steel plate shear walls. Two 10-story CoSPSW structures were designed using the proposed PBSD method and the traditional method respectively, and finite element models of both CoSPSW structures were constructed with ABAQUS (SIMULIA, 2014). Nonlinear pushover analyses and dynamic time-history analyses were carried out on both models and structural performances were compared to validate the effectiveness of the PBSD method. Incremental Dynamic Analyses (IDA) were also conducted, through which the seismic vulnerability of both CoSPSW structures was assessed probabilistically, and structural and nonstructural fragility curves were obtained.

2. PBSD Method for CoSPSW

In the PBSD process, inelastic structural performance will be fully considered. Therefore, the lateral load-carrying mechanism and lateral capacity of corrugated wall plate will be studied first, and the lateral strength formula will be provided. An ideal yield mechanism and target drift will then be identified, followed by the design base shear formula derived from energy conservation principle, with modifications accounting for the lateral load-carrying mechanism of corrugated wall plates involving both tension field action and in-plane shear-buckling. The inelastic lateral force distribution mode will be proposed, which would reflect the inelastic structural response of CoSPSWs. In the end, plastic design method of the corrugated wall plates and boundary frame members will be proposed to achieve the ideal yield mechanism and target drift.

2.1 Lateral Loading-Carrying Mechanism of Corrugated Wall Plates

Unlike flat wall plates in traditional SPSWs, the lateral load-carrying mechanism of corrugated wall plates involves both tension field action and in-plane shear-buckling (Qiu et al, 2018), as shown in Fig. 3 below. Due to corrugation, corrugated wall plates have much higher in-plane shear buckling strength than the flat wall plates, and usually involve inelastic buckling instead of elastic buckling. Therefore, the shear bucking strength τ_{cr} is non-negligible and should be considered in the lateral strength of corrugate wall plates, as shown in Eq. (1) below, which is the summation of shear resistance through tension field action and in-plane shear-buckling:

$$\tau = \tau_{cr} + 0.5\,\sigma_{ty}\sin 2\alpha\,, \tag{1}$$

$$\tan^4\alpha = \frac{1+\dfrac{tl}{2A_c}}{1+th\left(\dfrac{1}{A_b}+\dfrac{h^3}{360 I_c l}\right)}\,, \tag{2}$$

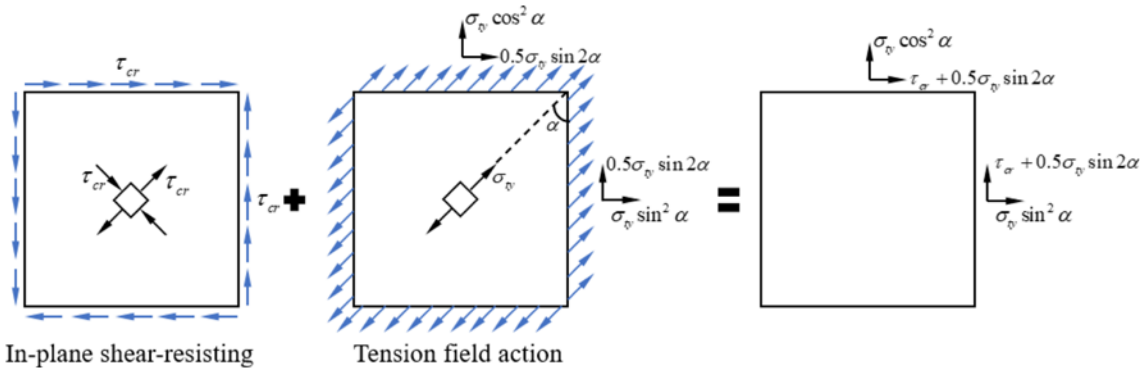

Fig. 3. Load-Carrying Mechanism of Corrugated Wall Plates

where τ_{cr} is the inelastic shear buckling stress of corrugated wall plates; σ_{ty} is the principal tensile stress caused by tension field action; α is the tension field inclination angle, assuming that it mainly depends on the anchoring affects provided by the boundary frame members (ANSI/AISC 341-16, 2016); h is the distance between the centerlines of the boundary beams; l is the distance between the centerlines of the boundary columns; t is the thickness of the wall plate; I_c, A_b and A_c are the column flexural rigidity, beam cross-sectional area and column cross-sectional area respectively.

For corrugated wall plates, inelastic shear buckling should be considered, and the inelastic shear buckling stress τ_{cr} can be calculated using Eq. (3) below (Zhao and Li, 2016). The inelastic shear buckling stress of the corrugated wall plates depends on their elastic shear buckling stress, which can be regarded as the interactive shear buckling stress conservatively, and calculated using the correlation formula of the local shear buckling stress and global shear buckling stress shown as Eqs. (5) – (8) below:

$$\tau_{cr} = \begin{cases} \tau_y & \lambda_s < 0.6 \\ \left[1 - 0.614(\lambda_s - 0.6)\right] \cdot \tau_y & 0.6 \le \lambda_s \le \sqrt{2} \\ \tau_y / \lambda_s^2 & \lambda_s > \sqrt{2}, \end{cases} \tag{3}$$

$$\lambda_s = \sqrt{\frac{\tau_y}{\tau_{cr,I}^e}}, \tag{4}$$

$$\left(\frac{1}{\tau_{cr,I}^e}\right)^2 = \left(\frac{1}{\tau_{cr,L}^e}\right)^2 + \left(\frac{1}{\tau_{cr,G}^e}\right)^2, \tag{5}$$

$$\tau_{cr,L}^e = \left(5.34 + \left(\frac{b}{l_n}\right)^2\right) \frac{\pi^2 E}{12(1-\nu^2)} \left(\frac{t}{b}\right)^2, \tag{6}$$

$$\tau_{cr,G}^e = k_G \frac{D_s^{0.75} D_w^{0.25}}{t l_n^2}, \tag{7}$$

$$k_G = 40 + 100 \frac{a^2}{l_n t}, \tag{8}$$

where $\tau_{cr,L}^e$ and $\tau_{cr,G}^e$ are the local and global and interactive elastic shear buckling stress of the corrugated wall plate respectively (Zhao and Li, 2016); $\tau_{cr,I}^e$ is the interactive elastic shear buckling stress of the corrugated wall plate (Yi et al., 2008); E, ν and τ_y are the elastic modulus, Poisson's ratio and the shear yield strength of wall plate steel respectively; λ_s is the shear slenderness ratio of the corrugated wall plate; k_G is the global shear buckling coefficient of corrugated wall plates; D_s and D_w are the flexural rigidities of the corrugated wall plate about the strong and weak axes respectively; l_n is the clear span of the wall plate; b is the largest subpanel width of corrugated wall plates; a is the corrugation depth (from the neutral axis to peak).

For any yielding point on the corrugated wall plate, the principal tensile stress caused by tension field action σ_{ty} can be calculated from Eq. (9) below according to the Von-Mises yield criterion, in which τ_{cr} is the inelastic shear buckling stress and f_y is the uniaxial tensile yield strength of wall plate steel:

$$3\tau_{cr}^2 + 3\tau_{cr}\sigma_{ty}\sin 2\alpha + \sigma_{ty}^2 = f_y^2. \tag{9}$$

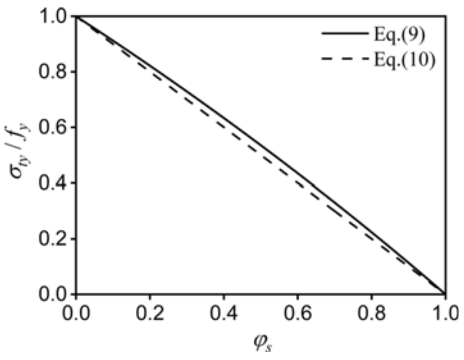

Fig. 4. Comparison of σ_{ty}

To avoid solving a quadratic equation, Eq. (9) is simplified into Eq. (10) below, and the difference is basically negligible, as shown in Fig. 4 below. Here φ_s is defined as the proportion coefficient of in-plane shear-buckling of corrugated wall plates.

$$\sigma_{ty} = (1 - \varphi_s) f_y \tag{10}$$

$$\varphi_s = \frac{\tau_{cr}}{\tau_y} \tag{11}$$

2.2 Yield Mechanism

Yield mechanism is an important performance objective for predicting and controlling the system seismic response, since it is closely related to the inelastic energy dissipation and reflects the failure process. A reasonable yield mechanism is an important prerequisite for the PBSD method of CoSPSWs. Based on experimental observations (Emami et al., 2013; Hosseinzadeh et al., 2017; Cao and Huang, 2018; Qiu et al., 2018), the ideal yield mechanism of CoSPSWs should involve yielding of all corrugated wall plates, and forming of plastic hinges at both ends of each boundary beam as well as base of boundary columns. In this ideal yield mechanism, most of the plastic deformations should concentrate in the corrugated wall plates and boundary beam ends, and the inter-story drifts should be uniformly-distributed along the building height.

2.3 Target Drift and Yield Drift

Target drift and yield drift are important parameters in PBSD, since they not only reflect the ductility of the structure, but also provide a basis for determining the design base shear (Bayat, 2010; Sullivan, 2013). The target drift could be determined according to the design requirements, and the yield drift could be obtained from a nonlinear pushover analysis, or estimated with formulas proposed below.

In order to obtain the yield drift, lateral deformations of CoSPSW at yielding are firstly analyzed. Similar to flat steel plate shear walls, lateral deformations of CoSPSWs consist of the shear deformation, which comes from deformation of the corrugated wall plate under shear and tension field action, as well as the

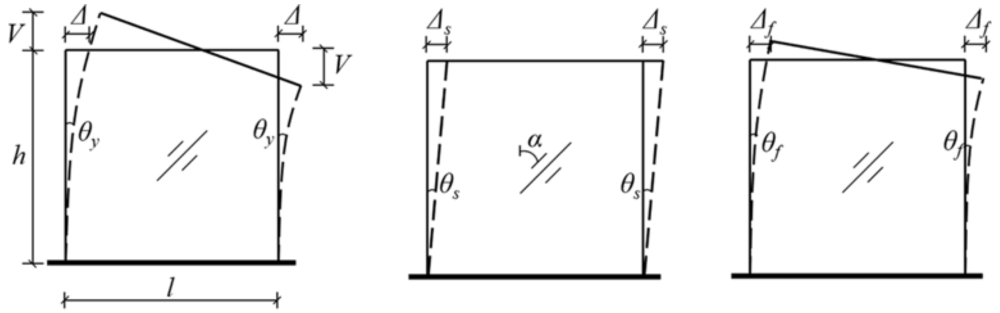

(a) (b) (c)

Fig. 5. Lateral Deformation of CoSPSWs: (a) Total Lateral Deformation, (b) Shear Deformation, (c) Bending Deformation

bending deformation, which comes from axial deformation of the columns (Bertero et al., 1991; Englekirk, 1994; Bayat, 2010), as shown in Fig. 5 below. Therefore, the yield drift θ_y consists of a shear component θ_s and a flexural component θ_f, as shown in Eq. (12):

$$\theta_y = \theta_s + \theta_f. \tag{12}$$

For the shear component θ_s, assuming that the boundary columns are axially rigid, and the lateral deformation mainly includes the shear deformation of the corrugated wall plate under in-plane shear and tension field action. Therefore, θ_s can be calculated according to Eq. (13):

$$\theta_s = \theta_{cr} + \theta_{TFA} = \frac{\tau_{cr}}{G} + \frac{2\sigma_{ty}}{E \cdot \sin 2\alpha}, \tag{13}$$

where θ_{cr} and θ_{TFA} are the drift under in-plane shear and tension field action respectively; G is the shear modulus of wall plate steel; τ_{cr} and σ_{ty} are the inelastic shear buckling stress and the principal tensile stress from tension field action of the wall plate respectively.

For the flexural component θ_f, CoSPSW is taken as a cantilever beam, and the lateral deformation mainly comes from axial deformation of the boundary columns. Axial buckling of the boundary columns is avoided, since the corrugated wall plates provide continuous lateral support with considerable out-of-plane flexural rigidity. The boundary columns could then act as the flanges of a cantilever beam, and CoSPSW can rotate due to the shortening of one column and the elongation of the other column. The stiffening effects of wall plates are ignored in this process, which is more accurate for corrugated wall plates due to "Accordion Effects". Therefore, θ_f can be calculated as Eq. (14):

$$\theta_f = \frac{\int_0^h \varepsilon dy}{l} = \frac{\varepsilon_{avg} h}{l} = \frac{\sigma_{avg}}{E}\frac{h}{l}, \tag{14}$$

where ε is the axial strain distribution in the boundary column along the story height; ε_{avg} is the average axial strain; σ_{avg} is the average axial stress.

In order to estimate a reasonable average axial stress, it is assumed that about 20% of the axial capacity of the boundary columns is utilized to resist the gravity loads (Bayat, 2010). The maximum axial stress ratio in columns could then be taken as 0.9, the upper limit given in the Chinese design standard (GB50017-2017, 2017), and the maximum axial stress ratio from lateral loads would be 0.72. If the section of the boundary column changes every several stories, the maximum axial stress ratio could be calculated for each story and the average axial stress would be obtained accordingly.

Nonlinear pushover analyses were conducted on 36 single-story CoSPSW models with different wall plate span, wall plate height, wall plate thickness, corrugation depth, as well as boundary beam and column sections, as shown in Table 1. The equivalent yield drift obtained from nonlinear pushover analysis with energy method ($\theta_{y,FEA}$) were compared to values calculated from the proposed formula in Eq. (12) ($\theta_{y,Eq}$), as shown in Fig. 6. The relative errors between the calculated values from Eq. (12) and the results from FEA pushover analyses have a mean value of 7.6% and a standard deviation of 0.27, while about 50% of the relative errors are within 10%. It is clear that yield drifts calculated from the proposed formulas were basically accurate and matched well with the FEA results, except for some CoSPSW models in which the corrugated walls had high shear slenderness ratio λ_s, probably due to the high out-of-plane deformation and more complex stress state of the walls. However, the formulas are still of practical significance and could provide a reference for structural design of CoSPSWs.

2.4 Design Base Shear

The design base shear could be calculated according to the energy conservation principle, which means if the structure is unidirectionally pushed to a target displacement, the work done by the external force is equal to the energy required for an equivalent elastoplastic single-degree-of-freedom (SDOF) system to reach the same state (Lee et al., 2004), as shown in Fig. 7 and Eq. (15) below:

$$\left(E_e + E_p\right) = \gamma\left(\frac{1}{2}MS_v^2\right) = \frac{1}{2}\gamma M\left(\frac{T}{2\pi}S_a g\right)^2, \tag{15}$$

$$\gamma = \frac{2\mu_s - 1}{R_\mu^2}, \tag{16}$$

where E_e and E_p are the elastic and plastic component of energy

Table 1. Models for the Yield Drift Calculation

No.	Wall plate			Corrugation depth (mm)	Boundary beam*	Boundary column*
	Span (mm)	Height (mm)	Thickness (mm)			
M1	3,000	3,000	4	20	H300×200×14×28	H400×400×12×24
M2	3,000	3,000	4	50	H250×150×8×10	H350×350×16×24
M3	3,000	3,000	4	80	H250×150×8×10	H350×350×16×24
M4	3,000	3,000	8	20	H350×250×18×28	H500×500×18×24
M5	3,000	3,000	8	50	H300×200×10×20	H400×400×12×24
M6	3,000	3,000	8	80	H300×200×10×20	H350×350×16×24
M7	3,000	3,000	16	20	H400×300×20×32	H500×500×28×42
M8	3,000	3,000	16	50	H250×150×8×10	H400×400×16×24
M9	3,000	3,000	16	80	H300×200×10×20	H400×400×16×32
M10	3,600	3,600	4	20	H350×250×18×28	H450×450×16×32
M11	3,600	3,600	4	50	H300×200×10×20	H400×400×12×24
M12	3,600	3,600	4	80	H250×150×8×10	H350×350×16×24
M13	3,600	3,600	8	20	H400×300×20×36	H500×500×30×42
M14	3,600	3,600	8	50	H300×200×14×28	H350×350×16×28
M15	3,600	3,600	8	80	H250×150×8×10	H350×350×16×24
M16	3,600	3,600	16	20	H500×400×24×36	H600×600×40×52
M17	3,600	3,600	16	50	H300×200×14×28	H450×450×16×32
M18	3,600	3,600	16	80	H300×200×10×20	H450×450×16×32
M19	4,500	3,000	4	20	H450×350×16×30	H500×500×18×36
M20	4,500	3,000	4	50	H350×250×18×28	H400×400×16×32
M21	4,500	3,000	4	80	H300×200×14×28	H350×350×16×24
M22	4,500	3,000	8	20	H500×450×18×36	H650×650×24×42
M23	4,500	3,000	8	50	H400×300×20×32	H500×500×18×36
M24	4,500	3,000	8	80	H300×200×10×20	H400×400×12×24
M25	4,500	3,000	16	20	H700×500×28×42	H700×700×36×54
M26	4,500	3,000	16	50	H450×350×16×32	H500×500×36×48
M27	4,500	3,000	16	80	H350×250×18×28	H450×450×16×32
M28	5,400	3,600	4	20	H500×400×16×32	H500×500×30×42
M29	5,400	3,600	4	50	H400×300×20×32	H500×500×18×36
M30	5,400	3,600	4	80	H350×250×18×28	H400×400×16×32
M31	5,400	3,600	8	20	H700×450×26×36	H650×650×36×54
M32	5,400	3,600	8	50	H500×400×16×32	H500×500×36×48
M33	5,400	3,600	8	80	H400×300×20×32	H500×500×18×36
M34	5,400	3,600	16	20	H700×600×40×54	H800×800×56×64
M35	5,400	3,600	16	50	H600×450×26×36	H650×650×36×54
M36	5,400	3,600	16	80	H400×300×20×32	H500×500×18×36

*Note: H sections: overall depth (mm) × flange width (mm) × web thickness (mm) × flange thickness (mm).

required to achieve the target displacement respectively; S_a is spectral acceleration; S_v is the design pseudo-velocity; T is the fundamental period of CoSPSW (Zhao et al., 2020); M is the equivalent total mass of the structure; g is the gravitational acceleration; γ is the energy correction factor (Lee et al., 2004); μ_s and R_μ are the ductility coefficient and ductility reduction coefficient respectively (Newmark and Hall, 1982).

The elastic and plastic component of the energy E_e and E_p are energy dissipated through elastic and inelastic deformation of structural components respectively, and obtained from Eqs. (17) and (18) below (Bayat, 2010):

$$E_e = \frac{1}{2} M \left(\frac{T}{2\pi} \frac{V_y}{W} g \right)^2 , \tag{17}$$

$$E_p = V_y \left(\sum_{i=1}^{n} \lambda_i H_i \right) \theta_p , \tag{18}$$

$$\theta_p = \theta_u - \theta_y . \tag{19}$$

where V_y is the design base shear; λ_i is the lateral force distribution coefficient of i^{th} story, which will be illustrated in the next section; W is the representative value of the total gravity load of

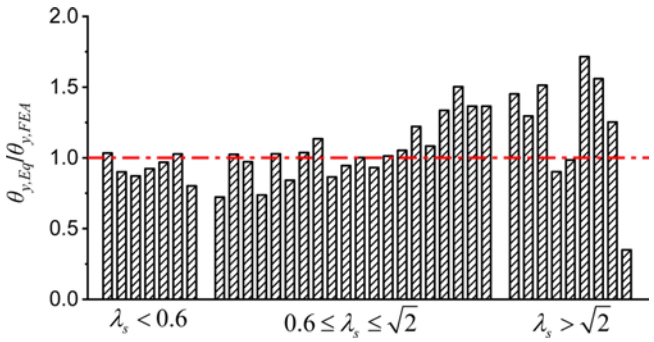

Fig. 6. Comparison of Yield Drift θ_y

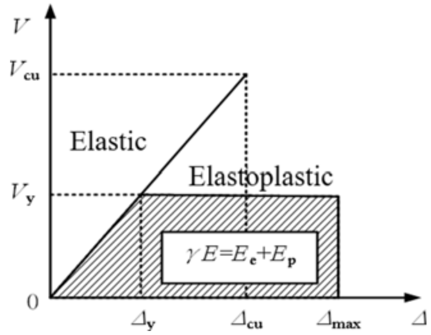

Fig. 7. Effective Energy Balance Concept

the structure; H_i is the altitude of the i^{th} floor; n is the total number of stories; θ_p is the plastic drift; θ_u is the target drift; θ_y is the yield drift obtained from Eq. (12).

By substituting Eqs. (17) and (18) into Eq. (15), the design base shear could be obtained from Eq. (20):

$$V_y = \frac{-\alpha_s + \sqrt{\alpha_s^2 + 4\gamma S_a^2}}{2} W , \tag{20}$$

$$\alpha_s = \sum_{i=1}^{n} (\lambda_i H_i) \frac{\theta_p 8\pi^2}{T^2 g} . \tag{21}$$

2.5 Inelastic Lateral Force Distribution Mode

In the current design specifications, the lateral force distribution mode is determined assuming an elastic structural response, while as the structure enters the inelastic state under rare earthquakes, the lateral force distribution mode might change significantly from the original assumptions, which might lead to unpredictable structural failure. Therefore, a lateral force distribution mode that reflects the inelastic structural response under earthquakes was proposed for CoSPSWs (Zhao, 2018), in which the elastic lateral force distribution formulas in the Chinese seismic design specification (GB50011-2010, 2010) was modified by calibrating the coefficient δ_n through nonlinear time-history analyses on 5-, 10-,15- and 20-story CoSPSW models under rare earthquakes. The lateral force F_i of i^{th} story is then shown below:

$$F_i = \lambda_i V_y , \tag{22}$$

$$V_i = \sum_{j=i}^{n} \lambda_i V_y = \frac{\sum_{j=i}^{n} W_j H_j}{\sum_{j=1}^{n} W_j H_j} V_y \left(1 - \delta_n\right) + \delta_n V_y , \tag{23}$$

$$V_n = \lambda_n V_y = \frac{W_n H_n}{\sum_{j=1}^{n} W_j H_j} V_y \left(1 - \delta_n\right) + \delta_n V_y , \tag{24}$$

$$\delta_n = 0.008T + 0.11 . \tag{25}$$

where W_j is the representative value of gravity load of i^{th} story; V_i and V_n are the story shear force of the i^{th} story and top story respectively; δ_n is the top additional seismic action coefficient.

The lateral force V_i should be further modified according to Eqs. (26) and (27) to consider the *P-Δ* effect:

$$V_i^* = V_i \left(1 + \theta_i\right) , \tag{26}$$

$$\theta_i = \frac{\sum_{j=i}^{n} W_j \Delta_i}{R_0 V_i h_i} , \tag{27}$$

where θ_i is the stability coefficient; R_0 is the super strength correction coefficient (Mitchell et al., 2003); Δ_i is the inter-story displacement of i^{th} story when the structure achieves the target drift.

In order to facilitate the calculation of story shear forces and the design of components, a dimensionless shear distribution coefficient β_i is defined as the ratio of the story shear force of the i^{th} story to the story shear force of the top story, as shown below:

$$\beta_i = \frac{V_i^*}{V_n} , \tag{28}$$

where β_i is the shear distribution coefficient of i^{th} story.

2.6 Design of Components

2.6.1 Corrugated Wall Plate

According to the ideal yield mechanism of CoSPSW shown in Fig. 2, the seismic energy is dissipated by the yielding of corrugated wall plates, as well as formation of plastic hinges at the ends of boundary beams and column bases. An energy balance equation could then be established as Eq. (29) below:

$$\sum_{i=1}^{n} F_i H_i \theta_p = \sum_{i=1}^{n} \left[\left(\tau_i t_i - \tau_{i+1} t_{i+1} \right) \theta_p l h_i \right] + 2 M_{pc} \theta_p + \sum_{i=1}^{n} 2 M_{pb,i} \theta_p , \tag{29}$$

where M_{pc} and $M_{pb,i}$ are the plastic moments at the column base and the beam end of i^{th} story respectively; h_i is the story height of i^{th} story; t_i and t_{i+1} are the wall plate thickness of i^{th} story and $(i+1)^{th}$ story, and when $i = n$, $t_{i+1} = 0$; τ_i and τ_{i+1} are the nominal shear strength of corrugated wall plate of i^{th} story and $(i+1)^{th}$ story, which can be calculated from Eq. (1).

In order to achieve a uniform distribution of plastic deformation along the building height and avoid a weak layer, the design shear capacity distribution of CoSPSW should be consistent with the inelastic story shear force distribution along the building height. Considering that only the bearing capacity of the wall plate is considered in the design of SPSWs (ANSI/AISC 341-16, 2016), the required thickness of corrugated wall plate for each story can be obtained as Eq. (30):

$$t_i = \beta_i t_n \,, \tag{30}$$

where t_n is the wall plate thickness of top story.

By substituting Eq. (30) into Eq. (29), the wall plate thickness of top story t_n could be obtained from Eq. (31) below, and the minimum required wall plate thickness t_i for each story could be determined accordingly.

$$t_n = \frac{\sum_{i=1}^{n} F_i H_i - 2M_{pc} - \sum_{i=1}^{n} 2M_{pb,i}}{\sum_{i=1}^{n} \left(\tau_i \beta_i - \tau_{i+1} \beta_{i+1}\right)} \,. \tag{31}$$

2.6.2 Design of Boundary Beams

According to the ideal yield mechanism of CoSPSW shown in Fig. 2, plastic hinges will form at the ends of boundary beams. A free body diagram of boundary beam at the i^{th} story with plastic hinges formed at both ends is shown in Fig. 8 below, in which $V_{l,i}$ and $V_{r,i}$ are the shear force at the left and right end of i^{th} story beam, $q_{bv1,i}$ and $q_{bv2,i}$ are the vertical distributed load at the lower and upper flange of i^{th} story beam, $q_{bh1,i}$ and $q_{bh2,i}$ are the horizontal distributed load at the lower and upper flange of i^{th} story beam, calculated from Eqs. (32) – (37). The boundary beam is designed as a flexural member following Chinese design standard (GB50017-2017, 2017) considering continuous lateral bracing from the floor slabs, and the shear bearing capacity of beam $V_{ub,i}$ at the i^{th} story is also checked to avoid shear failure:

$$V_{l,i} = \frac{2M_{pb,i}}{l_{n,i}} + \frac{\left(q_{bv2,i} - q_{bv1,i}\right) l_{n,i}}{2} + \frac{\left(q_{bh1,i} + q_{bh2,i}\right) l_{n,i}}{h_{b,i}} \,, \tag{32}$$

$$V_{r,i} = \frac{2M_{pb,i}}{l_{n,i}} + \frac{\left(q_{bv1,i} - q_{bv2,i}\right) l_{n,i}}{2} + \frac{\left(q_{bh1,i} + q_{bh2,i}\right) l_{n,i}}{h_{b,i}} \,, \tag{33}$$

$$q_{bv1,i} = \sigma_{ty,i} \cos^2 \alpha_i t_i \,, \tag{34}$$

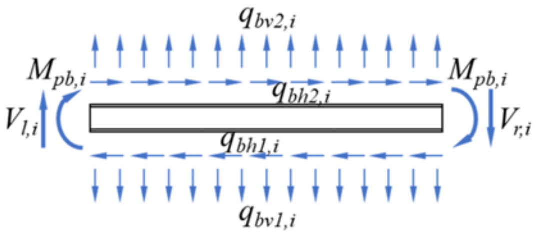

Fig. 8. Free Body Diagram of Boundary Beam

$$q_{bv2,i} = \sigma_{ty,i} \cos^2 \alpha_i t_{i+1} \,, \tag{35}$$

$$q_{bh1,i} = \tau_i t_i \,, \tag{36}$$

$$q_{bh2,i} = \tau_{i+1} t_{i+1} \,, \tag{37}$$

$$V_{ub,i} \geq \max\left(V_{l,i}, V_{r,i}\right) \,, \tag{38}$$

where $h_{b,i}$ is the cross-sectional height of i^{th} story beam; $l_{n,i}$ is the clear span of i^{th} story wall plate, $\sigma_{ty,i}$ is the principal tensile stress caused by tension field action of i^{th} story wall plate, α_i is the inclination angle of i^{th} story wall plate tension field.

For conventional SPSWs with flat wall plates, a minimum flexural rigidity of $I_{b,i} \geq 0.00307 \Delta t_i l^4 / h_i$ is required for each boundary beam at the i^{th} story, in order to ensure the full yielding of wall plates through tension field action (CAN/CSA S16-2014, 2014; ANSI/AISC 341-16, 2016), in which $\Delta t_i = t_i - t_{i+1}$. For CoSPSWs, since only partial tension field action is present in the corrugated wall plates, the minimum flexural rigidity could be modified and calculated as Eq. (39) below:

$$I_{b,i} \geq \left(1 - \varphi_{s,i}\right) \frac{0.00307 \Delta t_i l^4}{h_i} \,, \tag{39}$$

where $\varphi_{s,i}$ is the proportion coefficient of in-plane shear-buckling of i^{th} story wall plate.

2.6.3 Design of Boundary Columns

According to the ideal yield mechanism of CoSPSW shown in Fig. 2, the free body diagram of the i^{th} story boundary column is shown in Fig. 9, in which $N_{t,i}$ and $N_{b,i}$ are the axial force at the upper and lower end of i^{th} story column, $M_{b,i}$ and $M_{t,i}$ are the bending moment at the lower and upper end of i^{th} story column obtained from the inflection-point method, $V_{t,i}$ and $V_{b,i}$ are the shear force at the upper and lower end of i^{th} story column, $q_{cv,i}$ and $q_{ch,i}$ are the vertical and horizontal distributed load at the inner flange of i^{th} story column, calculated from Eqs. (40) – (43).

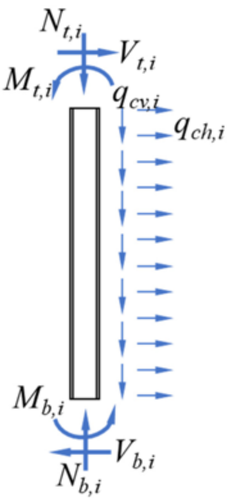

Fig. 9. Free Body Diagram of Boundary Column

The boundary column is designed as a compression-flexural or tension-flexural member following Chinese design standard (GB50017-2017, 2017), and the shear bearing capacity of column $V_{uc,i}$ at the i^{th} story is also checked to avoid shear failure:

$$V_{t,i} = \frac{M_{t,i}+M_{b,i}}{h_{n,i}} + \frac{q_{ch,i}h_{n,i}}{2}, \tag{40}$$

$$V_{b,i} = \frac{M_{t,i}+M_{b,i}}{h_{n,i}} - \frac{q_{ch,i}h_{n,i}}{2}, \tag{41}$$

$$q_{ch,i} = \sigma_{ty,i}\sin^2\alpha_i t_i, \tag{42}$$

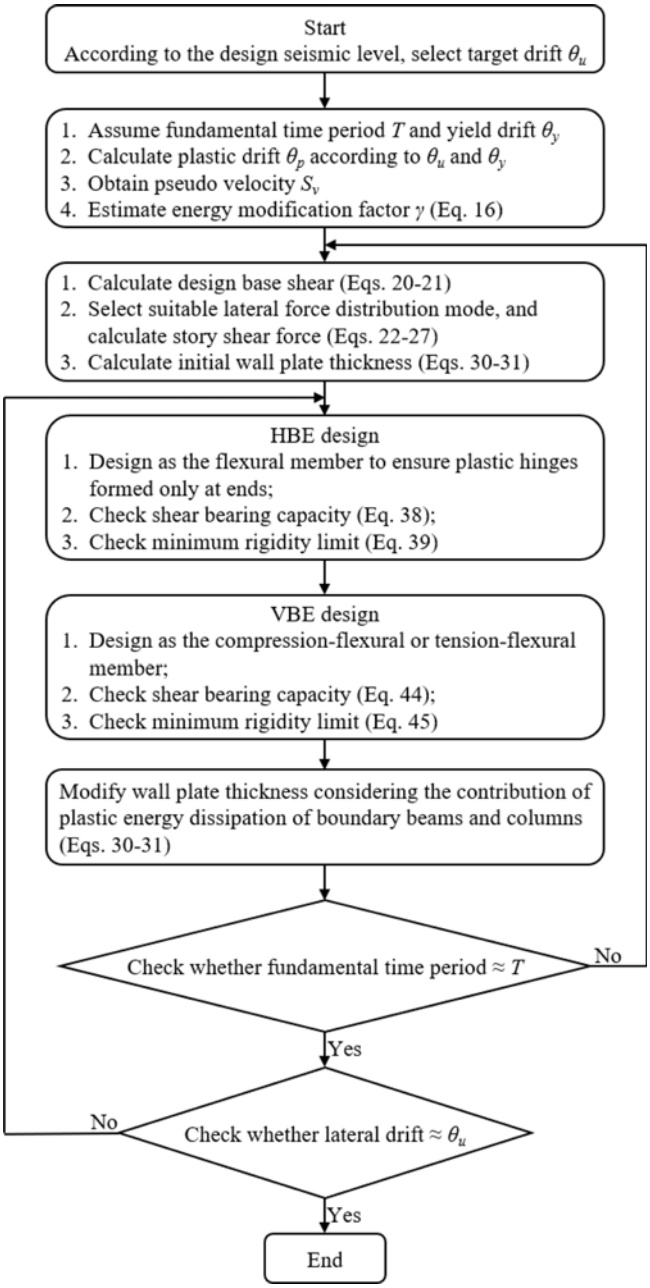

Fig. 10. Flowchart for the Proposed PBSD Method of CoSPSW

$$q_{cv,i} = \tau_i t_i, \tag{43}$$

$$V_{uc,i} \ge \max(V_{t,i}, V_{b,i}), \tag{44}$$

where $h_{n,i}$ is the clear height of i^{th} story wall plate.

For conventional SPSWs with flat wall plates, a minimum flexural rigidity of $I_{c,i} \ge 0.00307 t_i h_i^4/l$ is also required for each boundary column at the i^{th} story, in order to ensure the full yielding of wall plates through tension field action (CAN/CSA S16-2014, 2014; ANSI/AISC 341-16, 2016). Similar with the boundary beam, the minimum flexural rigidity for the boundary column could be modified and calculated as Eq. (45) below:

$$I_{c,i} \ge \left(1-\varphi_{s,i}\right)\frac{0.00307 t_i h_i^4}{l}. \tag{45}$$

A flow-chart is provided in Fig. 10, which shows the main steps of the PBSD method of CoSPSWs discussed in this section.

3. Validation of the Proposed PBSD Method

3.1 Design of CoSPSWs

Two 10-story CoSPSWs with a span of 4.5m and a story height of 3.2 m were designed with the proposed PBSD method and the traditional method respectively. The floor plan is shown in Fig. 11. The dead (live) load was 4.0 (2.0) kN/m^{2}on the floors, and 4.5 (2.0) kN/m^2 on the roof. The construction site is Class II (i.e., medium stiff soil) within a region of Seismic Intensity 8 and Design Earthquake Group I (GB 50011-2010, 2010). The floor was 120 mm thick cast-in-place concrete, and the beams and columns were steel welded H-sections with rigid beam-column connections. Q235B grade steel (235 MPa design yield strength) and Q345B grade steel (345 MPa design yield strength) were used for the corrugated wall plates and frame members respectively. The corrugation depth and wavelength of corrugated wall plate were 100 mm and 400 mm respectively, and the width of the subpanels were uniform. For the proposed PBSD method, the target drift θ_u was selected as 0.025 (ASCE/SEI 41-17, 2017), and the design parameters are shown in Table 2. Member sections

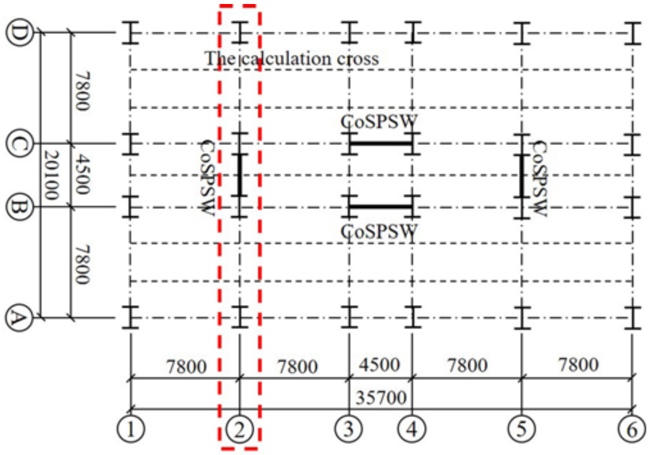

Fig. 11. Floor Plan of the Structure

Table 2. Design Parameters for PBSD

Design parameter	Value
Horizontal seismic influence factor	0.463
Spectral acceleration S_a/g	1.106
Fundamental period T/s	1.152
Yield drift θ_y	0.005
Target drift θ_u	0.025
Ductility coefficient μ_s	5
Ductility reduction coefficient R_μ	5
Energy correction factor γ	0.360
ξ	2.745
V_y/W	0.152

determined from the PBSD method and the traditional method are shown in Table 3.

3.2 Finite Element Models

Two 3-span CoSPSW structures with CoSPSW in the interior span and moment frames in the exterior spans were modeled using finite element software ABAQUS (SIMULIA, 2014), as shown in Fig. 12. Both frame beams and columns were modeled using beam element B31, while corrugated wall plates were simplified into equivalent braces (Jiang et al., 2019) and modeled by truss element T3D2, according to the principle of equivalent lateral stiffness and strength. The area A_{eb} and yield strength f_{eb} of the equivalent brace were calculated from Eqs. (46) and (48) respectively (Jiang et al., 2019). Out-of-plane displacements were restrained at all beam-column joints, and the columns were fixed at the base. A bilinear elastoplastic constitutive model considering strain hardening was adopted for the steel material of infill wall plate and boundary members with an elastic modulus E = 206 GPa, a strain hardening modulus E_h = 0.01E, a Poisson's ratio ν = 0.3, and a yield strength of 235 MPa and 345 MPa, respectively.

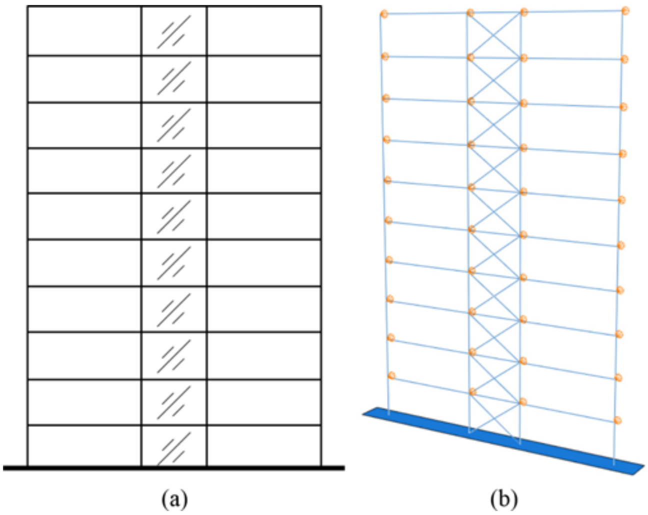
(a)
(b)

Fig. 12. Finite Element Model: (a) 3-Span CoSPSW Structure, (b) Finite Element Model

$$A_{eb} = \frac{K_P l_{eb}}{2E\cos^2\beta}, \tag{46}$$

$$K_P = \frac{0.95 E q_{co} l_n t}{2 h s_{co}(1+\nu)}, \tag{47}$$

$$f_{eb} = \frac{\tau_{cr} l_n t}{2A_{eb}\cos\beta}, \tag{48}$$

where l_{eb} is the length of the equivalent brace; q_{co} and s_{co} are the wavelength and corrugation developed length, respectively.

Verification analyses were firstly conducted in order to validate the modeling. Since currently no shaking-table tests have been conducted to CoSPSWs, a refined FEA model was constructed for the CoSPSW specimen of cyclic tests conducted by Emami et al. (2013), and time-history analysis was conducted and compared to test results, as shown in Fig. 13. It is clear that the hysteretic

Table 3. Member Sections from the PBSD Method and the Traditional Method

Model	Floor	Columns in the CoSPSW span*	Columns outside the CoSPSW span*	Wall plate thickness (mm)
Traditional method	7 – 10	H500×500×20×26	H400×400×16×20	3.0
	4 – 6	H600×600×30×38	H500×500×24×28	4.0
	1 – 3	H700×700×50×58	H600×600×28×36	5.0
PBSD method	10	H450×450×12×20	H350×350×16×18	1.8
	9	H500×500×14×22	H400×400×16×18	3.0
	8	H550×550×18×26	H400×400×16×20	4.0
	7	H600×600×24×32	H450×450×16×22	4.9
	6	H600×600×32×42	H450×450×20×26	5.6
	5	H650×650×36×48	H500×500×20×26	6.3
	4	H650×650×48×56	H500×500×24×28	6.9
	3	H700×700×48×56	H550×550×24×28	7.3
	2	H750×750×56×64	H550×550×28×32	7.6
	1	H750×750×68×72	H600×600×28×36	7.8

*Note: H sections: overall depth (mm) × flange width (mm) × web thickness (mm) × flange thickness (mm).

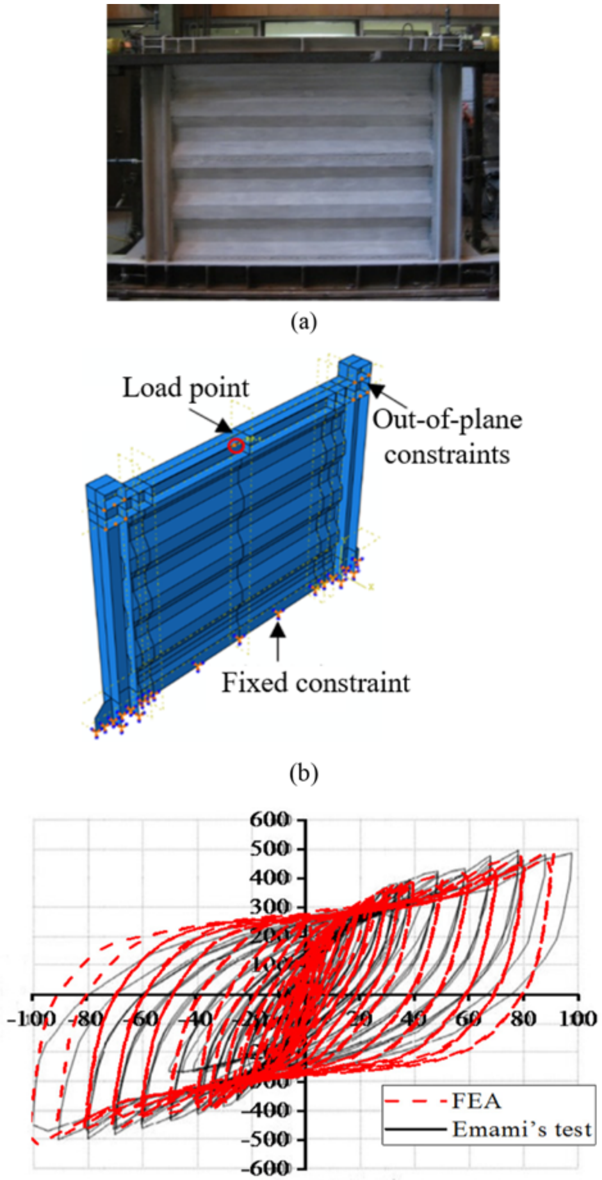

(a)

(b)

(c)

Fig. 13. Validation of Nonlinear Cyclic Analysis of CoSPSW Finite Element Model: (a) Test Specimen, (b) FEA Model, (c) Comparison of Results

curves obtained from FEA matched well with the test curves. Moreover, the simplified equivalent brace model was verified by comparing the time-history analysis response of a refined FEA model well as a simplified equivalent brace FEA model of a three-story CoSPSW structure under rare earthquake excitation, as shown in Fig. 14. It is clear that the time history curves obtained by the refined and simplified model coincide basically, especially near the peak value. Therefore, the simplified equivalent brace model was validated and adopted for subsequent analyses.

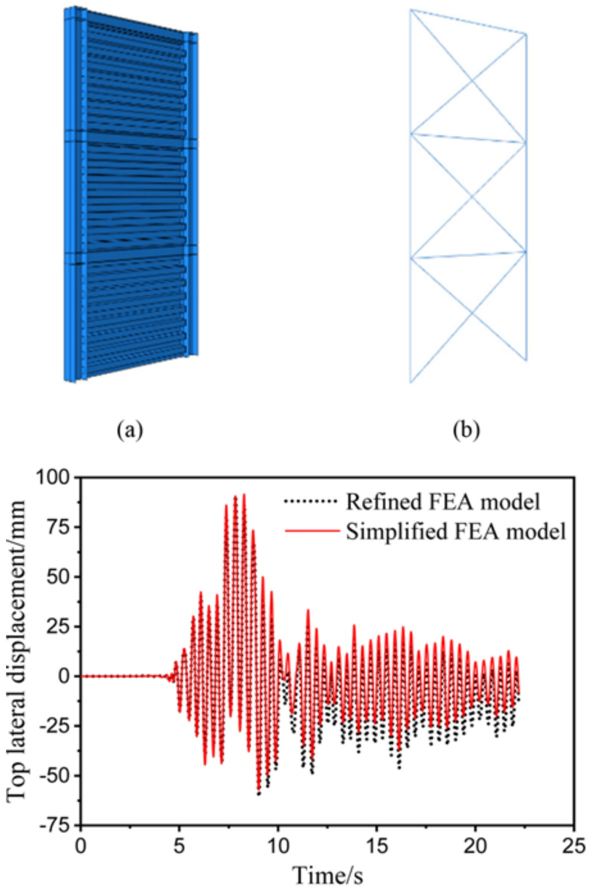

(a)

(b)

(c)

Fig. 14. Validation of Time-History Analysis of Simplified FEA Model of CoSPSW: (a) Refined Model, (b) Simplified Model, (c) Comparison of Results

3.3 Pushover Analysis

Nonlinear static pushover analyses were carried out on the CoSPSW structure model designed with the PBSD method to study its inelastic structural performance. A linear multi-point constraint (SIMULIA, 2014) was applied to a set of reference points, including a loading point and one point on each story of the model. Following the virtual work principles, the multi-point constraint should satisfy Eq. (49) below (Huang et al., 2011), to guarantee that during the pushover analysis, the story shear would always satisfy the proposed lateral force distribution mode. By substituting Eq. (28) into Eq. (49), the multi-point constraint could be simplified into Eq. (50) using the shear distribution coefficient β_i. A lateral displacement was calculated from Eq. (50) and applied to the loading point, which was corresponding to an overall drift of 2.5%, to ensure that the CoSPSW structure has well entered the inelastic stage.

$$\sum_{i=1}^{10}\left(F_i d_i\right)-\left(\sum_{i=1}^{10} F_i\right) d_0 = 0\,, \tag{49}$$

$$\sum_{i=2}^{10}\left[\left(\beta_{i-1}-\beta_i\right) d_i\right]+d_{10}=\beta_1 d_0\,, \tag{50}$$

where d_i is the lateral displacement of the i^{th} story; d_0 is the lateral displacement of the loading point.

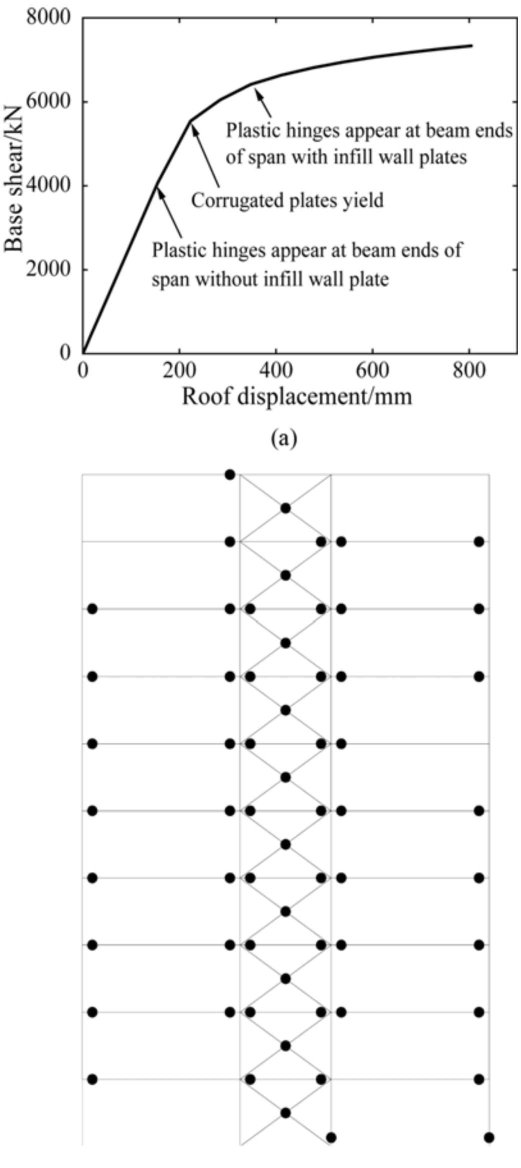

(b)

Fig. 15. Pushover Analysis of CoSPSW Structure Designed with PBSD Method: (a) Lateral Load-Displacement Curve, (b) Plastic Hinge Distribution

Figure 15(a) shows the lateral load-displacement curve from the pushover analysis, and Fig. 15(b) shows the distribution of plastic hinges at 2.5% lateral drift. During the pushover analysis, plastic hinges firstly appeared at the ends of the beams in the exterior span, and then the corrugated wall plates yielded gradually. As the lateral displacement continued to increase, plastic hinges started to appeared at the ends of the beams in the interior span, and finally at column bases, which was basically consistent with the expected yield mechanism. Therefore, the PBSD method proposed in this paper could predict and control the inelastic behavior of the designed CoSPSW structure relatively well.

3.4 Time-History Analyses

Nonlinear dynamic time-history analyses were carried out on both CoSPSW structure models, in order to study their seismic performance. Additional masses were applied at all the beam-column joints, and the earthquake excitation was input through the base. As shown in Table 4, ten earthquake excitation records with different spectrum characteristics were selected for the nonlinear time-history analyses. According to the Chinese seismic design specification (GB 50011-2010, 2010), the magnitudes of the earthquakes were all higher than 6.5, the effective periods were larger than 4s, and the peak ground acceleration (PGA) were adjusted to 0.51g.

Table 4. Selected Ground Motions

Record No.	Record	Minimum frequency (Hz)	PGA (g)	PGV* (cm/s)
RSN0169	IMPVALL.H_H-DLT352	0.09	0.35	33
RSN0174	IMPVALL.H_H-E11230	0.10	0.38	45
RSN0752	LOMAP_CAP090	0.25	0.51	38
RSN0767	LOMAP_G03090	0.13	0.56	45
RSN0953	NORTHR_MUL279	0.15	0.49	67
RSN0960	NORTHR_LOS270	0.13	0.47	41
RSN1111	KOBE_NIS090	0.13	0.48	47
RSN1485	CHICHI_TCU045N	0.05	0.51	46
RSN1602	DUZCE_BOL090	0.06	0.81	66
RSN1787	HECTOR_HEC090	0.04	0.33	45

*Note: PGV: peak ground velocity

For the CoSPSW structure designed with the PBSD method, the envelope curves of the shear distribution coefficient β_i from the time-history analyses are shown in Fig. 16, and compared to the shear distribution coefficient β_i calculated from Eq. (28) in the proposed PBSD method. The relative errors between the calculated values from Eq. (28) and the average values of envelope curves from the time-history analyses have a mean value of 12.7% and a standard deviation of 0.08, while about 60% of the relative errors are within 10%. As shown in Fig. 16, the shear distribution coefficient β_i adopted by the PBSD method matches relatively well with the time-history analysis results, which

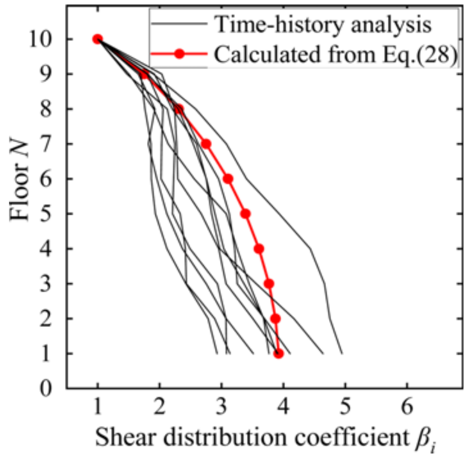

Fig. 16. Distribution of Story Shear Force

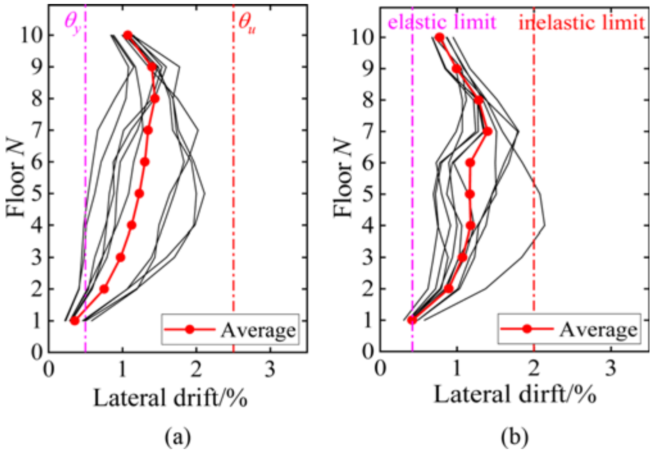

(a) (b)

Fig. 17. Inter-Story Drift under Seismic Excitations: (a) CoSPSW Structure Designed with the PBSD method, (b) CoSPSW Structure Designed with the Traditional Method

means that the lateral force distribution mode in the proposed PBSD method could reflect the inelastic state of the structure.

Figure 17 shows the envelope curves of inter-story drifts of the two CoSPSW structures under each seismic excitation, as well as the average values. According to the Chinese seismic design code (GB 50011-2010, 2010), inter-story drifts should not exceed an elastic drift limit of 1/250 and an inelastic drift limit of 1/50, under frequent and rare earthquakes respectively. As shown in Fig. 17, the inter-story drifts of some of the middle stories of the CoSPSW structure designed with the traditional method have exceeded the limit of 1/50 under rare earthquakes, and the inter-story drifts are unevenly distributed along the height of the building, with a potential weak layer at the building mid-height. On the other hand, all inter-story drifts of the CoSPSW structure designed with the PBSD method are well below the target drift θ_u of 2.5%, and distribute more smoothly along the building height.

From the pushover and time-history analyses on 10-story CoSPSW structures, it is clear that for the CoSPSW structure designed with the PBSD method, the corrugated wall plates and the boundary beams of each story have all participated effectively in energy dissipation, and the ideal yield mechanism was formed. All inter-story drifts were well below the target drift θ_u of 2.5%, and distributed more smoothly along the building height, which helped to avoid potential weak layers. Therefore, the effectiveness of the proposed PBSD method was validated.

4. Probabilistic Assessment of the CoSPSW Structures

4.1 Fragility Function Methodology

The seismic performance and vulnerability of both CoSPSW structures were further assessed through the probabilistic assessment, which estimated the probabilistic structural response, herein termed as the engineering demand parameter (EDP), as a function of ground motion intensity, herein termed as the intensity measure (IM), and used quantitative measures to evaluate the structural and nonstructural performance under seismic loads (Zhang and Zirakian, 2015; Esteghamati et al., 2020; Esteghamati and Farzampour, 2020a; Esteghamati and Farzampour, 2020b). The probabilistic seismic demand model (PSDM) was employed to relate EDPs to IMs and derive the fragility functions, through Incremental Dynamic Analysis (IDA) of the CoSPSW structure models in which the PGAs were scaled to different intensity levels (Zhang and Zirakian, 2015). The conditional mean and standard deviation of EDP for a given IM were estimated by regression analysis, and the relationship between the mean EDP and IM is as follows:

$$EDP = a(IM)^b \text{ or } \ln(EDP) = b\ln(IM) + \ln(a) , \tag{51}$$

where constants a and b are regression coefficients obtained from regression analysis. It is assumed that the remaining variability in ln(*EDP*) for a given IM has a constant variance for all IMs, and the standard deviation can be obtained as follows (Baker and Cornell, 2006):

$$\zeta_{EDP|IM} = \sqrt{\frac{\sum_{i=1}^{N}\left[\ln(EDP_i) - \ln\left(a(IM_i)^b\right)\right]^2}{N-2}} , \tag{52}$$

where N is the number of EDP-IM data pairs, and EDP_i and IM_i are the values of the i^{th} pair. Assuming that EDP has a lognormal distribution for a given IM, the fragility function defining the probability of EDP reaching or exceeding a certain limit state (LS) under a given IM is as follows:

$$P(EDP \geq LS|IM) = 1 - \int_0^{LS} \frac{1}{\sqrt{2\pi}\cdot\zeta_{EDP|IM}\cdot EDP} \cdot e^{\left[-\frac{1}{2}\left(\frac{\ln(EDP)-\ln\left(a(IM)^b\right)}{\zeta_{EDP|IM}}\right)^2\right]} \cdot d(EDP) \tag{53}$$

Accordingly, ln(EDP) can be considered to have a standard normal distribution, and Eq. (53) could be simplified into the following equation, using the standard normal cumulative distribution function Φ(·):

$$P(EDP \geq LS|IM) = 1 - \Phi\left(\frac{\ln(LS) - \ln\left(a(IM)^b\right)}{\zeta_{EDP|IM}}\right) . \tag{54}$$

4.2 Fragility Curves of the CoSPSW Structures

IDA analyses were conducted on both CoSPSW structures with the seismic excitations in Table 4, the PGA of which was adjusted to 0.1 g to 1.2 g, with an interval of 0.1 g. Peak inter-story drift and PGA were selected as the EDP and IM respectively in this study, since inter-story drift is an important demand measure and used for the seismic loss estimation methodology provided by Federal Emergency Management Agency (FEMA) (HAZUS-MH MR5, 2010), and PGA has been adopted in developing fragility functions for various structures including SPSWs (Akkar et al., 2005; Yakut and Yilmaz, 2008; Zhang and

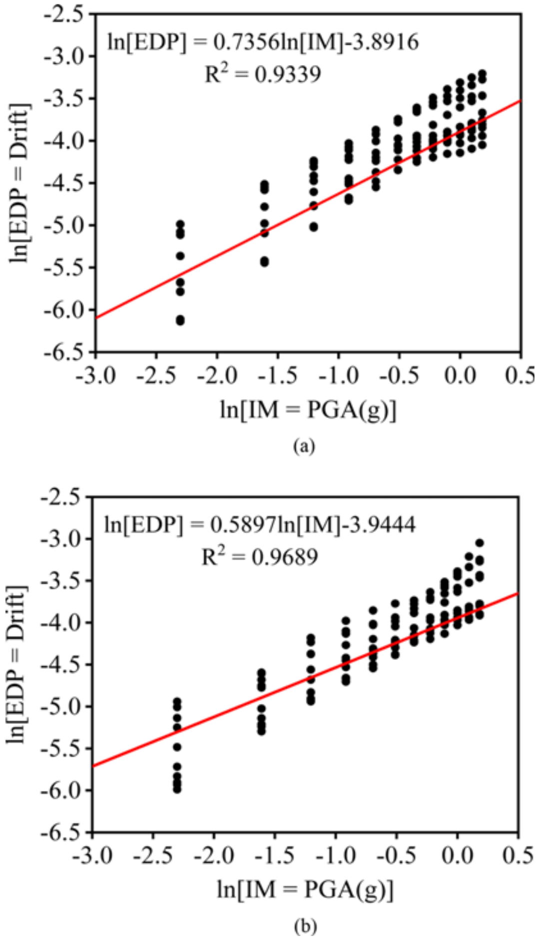

Fig. 18. Relationship between ln[IM] and ln[EDP]: (a) CoSPSW Structure Designed with the PBSD Method, (b) CoSPSW Structure Designed with the Traditional Method

Zirakian, 2015).

From the IDA analyses, a large number of peak inter-story drift and corresponding PGA, i.e., EDP-IM data pairs were obtained, and ln[IM = PGA] and ln[EDP = Drift] are plotted in Fig. 18. The linear regression equation and determination coefficient R^2 value were then obtained through linear regression analyses, as shown in Fig. 18. It is clear that the R^2 values for the CoSPSW Structures designed with the PBSD method and with the traditional method are 0.9339 and 0.9689, both of which are greater than 0.9, indicating that there was a strong correlation. Therefore, the Drift-PGA data pairs were appropriate to develop the fragility functions for CoSPSW structures. Accordingly, lognormal distribution parameters a and b, standard deviation and functional relation were determined, as shown in Table 5.

Table 6. Repair states of CoSPSWs

Repair states	Story drift	Description
RS1	0.002	Repair infill wall surface
RS2	0.008	Replace infill wall
RS3	0.01	Repair boundary beam and beam-column connection
RS4	0.018	Repair boundary column
RS5	0.043	Replace boundary beam, column or frame

Table 7. Nonstructural Damage States (HAZUS-MH MR5, 2010)

Damage states	Slight	Moderate	Extensive	Complete
Story drift	0.004	0.008	0.025	0.050

Another key issue in developing fragility functions is the definition of limit states, i.e., LS in the fragility function Eq. (54). Referring to the damage and repair states of SPSWs (Baldvins et al., 2012), the experimental results of CoSPSWs from literatures were reviewed and analyzed, and five repair states were proposed for CoSPSWs, according to the possible damage degree to the infill corrugated wall plate and boundary frame members under certain drift level (Zhao, 2018). The repair states and associated story drifts are listed in Table 6, which were adopted as limit states (LS) in the fragility function Eq. (54), to develop the structural fragility curves of the CoSPSW structures. In addition, according to HAZUS-MH MR5 (2010), damage states of the drift-sensitive nonstructural components were described by ‘Slight’, ‘Moderate’, ‘Extensive’, and ‘Complete’, respectively, as listed in Table 7 with associated story drifts, which were adopted as limit states to develop the nonstructural fragility curves of the CoSPSW structures. From the limit states described in Tables 6 and 7, structural and nonstructural fragility curves for both CoSPSW structures were developed through probabilistic seismic demand analysis, as shown in Figs. 19 and 20.

The seismic vulnerability of both CoSPSW structures were assessed by comparing the 25th percentile PGA values, i.e., PGA values corresponding to exceeding probability of 25%, of the fragility curves for all damage/repair states in Figs. 19 and 20. The 25th percentile PGA values obtained from the structural and nonstructural fragility curves are shown in Figs. 21 and 22.

It is clear from Figs. 21 and 22 that from RS1 to RS5 repair states and from “Slight” to “Complete” damage states, the 25th percentile PGA values for both CoSPSW structures increase significantly, indicating that the CoSPSW structure would experience

Table 5. Regression Coefficients, Standard Deviation and Functional Relation for EDP-IM Data Pairs

Design method	Selected		Regression coefficients		$\zeta_{EDP\|IM}$	Functional relation
	EDP	IM	a	b		
PBSD method	Drift	PGA	0.0204	0.7356	0.3234	$\text{Drift} = 0.0204(\text{PGA})^{0.7356}$
Traditional method	Drift	PGA	0.0194	0.5897	0.6612	$\text{Drift} = 0.0194(\text{PGA})^{0.5897}$

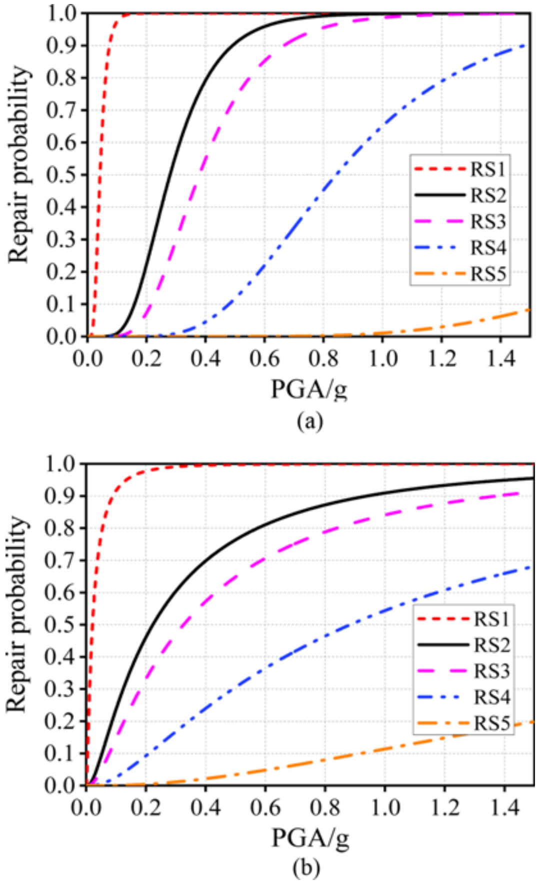

(a)

(b)

Fig. 19. Structural Fragility Curves: (a) CoSPSW Structure Designed with the PBSD Method, (b) CoSPSW Structure Designed with the Traditional Method

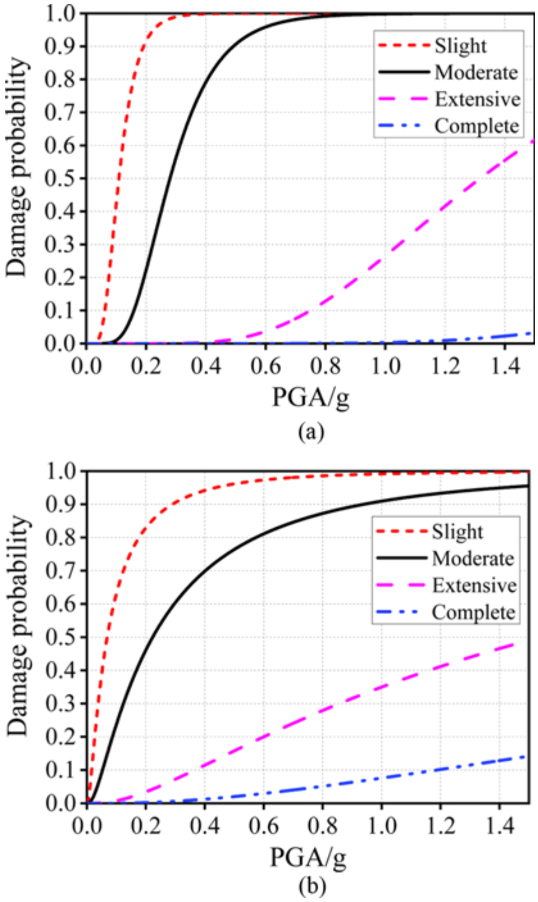

(a)

(b)

Fig. 20. Nonstructural Fragility Curves: (a) CoSPSW Structure Designed with the PBSD Method, (b) CoSPSW Structure Designed with the Traditional Method

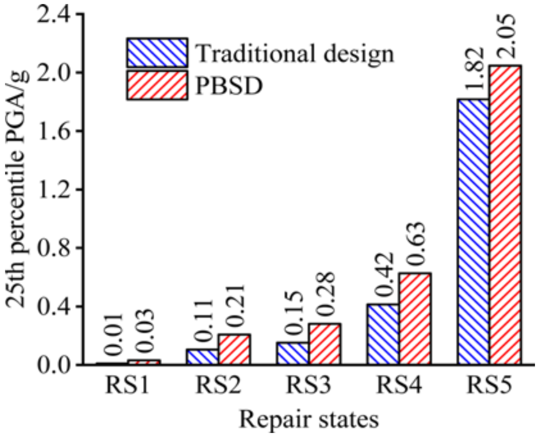

Fig. 21. The 25th Percentile PGA from Structural Fragility Curves

more serious damages with the increase of seismic intensity. Furthermore, for the structural repair state of RS1 to RS5, the 25th percentile PGA values of the fragility curves of the CoSPSW structure designed with the PBSD method are 220%, 98%, 84%, 51% and 13% higher than the CoSPSW structure designed with the traditional method, respectively. For the nonstructural damage state of Slight to Complete, the 25th percentile PGA values of the fragility curves of the CoSPSW structure designed with the PBSD method are 145%, 98%, 36%, and 7% higher than the CoSPSW structure designed with the traditional method, respectively. Therefore, CoSPSW structure designed with the PBSD method had lower seismic vulnerability as well as probability of nonstructural damage, i.e. better seismic performance, than the CoSPSW structure designed with the traditional method.

5. Conclusions

A performance-based seismic design (PBSD) method was proposed for corrugated steel plate shear walls (CoSPSWs). Two 10-story CoSPSW structures were designed with the proposed PBSD method and the traditional design method respectively, and nonlinear static pushover analyses and dynamic time-history analyses were conducted to validate the effectiveness of the PBSD method. A probabilistic assessment was carried out on the seismic vulnerability of both CoSPSW structures through Incremental Dynamic Analysis (IDA), and the structural and nonstructural fragility curves were obtained. The main conclusions were summarized as follows:

1. Ideal yield mechanism and target drift were selected as the two main performance objectives for the Performance-based seismic design (PBSD) method, with considerations

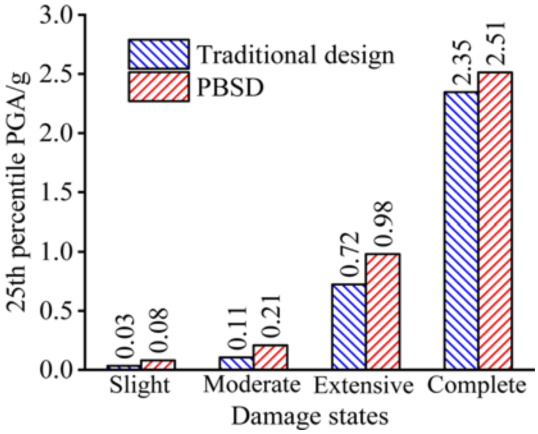

Fig. 22. The 25th Percentile PGA from Nonstructural Fragility Curves

of inelastic structural performance. The inelastic behavior and yield mechanism of CoSPSW structure designed with the PBSD method would be more controllable and predictable under the design earthquake.

2. Static pushover analyses revealed that CoSPSW structure designed with the PBSD method presented the ideal yield mechanism, and the development as well as final locations of plastic hinges were consistent with the design assumptions. The proposed PBSD method was able to predict and control the inelastic behavior of the CoSPSW structure relatively well.
3. Nonlinear dynamic time-history analyses revealed that all inter-story drifts in the CoSPSW structure designed with the PBSD method were well below the target drift θ_u of 2.5%, and distributed more smoothly along the building height, which helped to avoid potential weak layers in the middle stories. In addition, the lateral force distribution mode in the PBSD method matched relatively well with the time-history analysis results, indicating that it could reflect the inelastic state of the structure.
4. Structural and nonstructural fragility curves of both CoSPSW structures were obtained through probabilistic seismic demand analysis using incremental dynamic analyses, which showed that the 25th percentile PGA values of the CoSPSW structure designed with the PBSD method were 220%, 98%, 84%, 51% and 13% higher for the structural repair states of RS1 to RS5 respectively, and 145%, 98%, 36%, and 7% higher for the nonstructural damage states of Slight to Complete. Therefore, CoSPSW structure designed with the PBSD method had lower seismic vulnerability as well as lower probability of nonstructural damage, compared to CoSPSW structure designed with the traditional method.

Acknowledgments

The authors gratefully acknowledge the financial supports by the National Natural Science Foundation of China under Grant numbers No. 51878447, No. 51678406, and No. 51378340.

ORCID

Not Applicable

References

AISC (2016) Seismic provisions for structural steel buildings. ANSI/AISC 341-16, American Institute of Steel Construction, Chicago, IL, USA

Akkar S, Sucuoğlu H, Yakut A (2005) Displacement-based fragility functions for low- and mid-rise ordinary concrete buildings. *Earthquake Spectra* 21(4):901-927, DOI: 10.1193/1.2084232

ASCE (2017) Seismic evaluation and retrofit of existing buildings. ASCE/SEI 41-17, American Society of Civil Engineers, Reston, VA, USA

Bahrebar M, Kabir M, Zirakian M, Hajsadeghi M, Lim J (2016) Structural performance assessment of trapezoidally-corrugated and centrally-perforated steel plate shear walls. *Journal of Constructional Steel Research* 122:584-594, DOI: 10.1016/j.jcsr.2016.03.030

Bahrebar M, Lim J, Clifton G, Zirakian T, Shahmohammadi A, Hajsadeghi M (2020) Perforated steel plate shear walls with curved corrugated webs under cyclic loading. *Structures* 24:600-609, DOI: 10.1016/j.istruc.2020.01.047

Baker JW, Cornell CA (2006) Vector-valued ground motion intensity measures for probabilistic seismic demand analysis. PEER Report 2006/08, University of California, Berkeley, CA, USA

Baldvins NM, Berman JW, Lowes LN, Janes TM, Low NA (2012) Fragility functions for steel plate shear walls. *Earthquake Spectra* 28(2):405-426, DOI: 10.1193/1.4000003

Bayat MR (2010) Performance-based plastic design of earthquake resistant steel structures: Concentrically Braced Frames, Tall Moment Frames, Plate Shear Wall Frames. PhD Thesis, University of Texas at Arlington, Arlington, VA, USA

Berman JW (2011) Seismic behavior of code designed steel plate shear walls. *Engineering Structures* 33(1):230-244, DOI: 10.1016/j.engstruct.2010.10.015

Berman JW, Bruneau M (2003) Plastic analysis and design of steel plate shear walls. *ASCE-Journal of Structural Engineering* 129(11):1448-1456, DOI: 10.1061/(ASCE)0733-9445(2003)129:11(1448)

Berman JW, Bruneau M (2005) Experimental investigation of light-gauge steel plate shear walls. *Journal of Structural Engineering* 131:259-267, DOI: 10.1061/(ASCE)0733-9445(2005)131:2(259)

Bertero VV, Anderson JC, Krawinkler H, Miranda E (1991) Design guidelines for ductility and drift limits. Report No. UCB/EERC-91/15, University of California, Earthquake Engineering Center, Berkeley, CA, USA

Bhowmick AK, Grondin GY, Driver RG (2011) Estimating fundamental periods of steel plate shear walls. *Engineering Structures* 33(6):1883-1893, DOI: 10.1016/j.engstruct.2011.02.010

Cao Q, Huang J (2018) Experimental study and numerical simulation of corrugated steel plate shear walls subjected to cyclic loads. *Thin-Walled Structures* 127:306-317, DOI: 10.1016/j.tws.2018.01.042

Chao SH, Goel SC, Lee SS (2007) A seismic design lateral force distribution based on inelastic state of structures. *Earthquake Spectra* 23(3):547-569, DOI: 10.1193/1.2753549

CSA (2014) Design of steel structures. CAN/CSA-S16-2014, Canadian Standard Association, Mississauga, ON, Canada

Ding Y, Deng E, Zong L, Dai X, Lou N, Chen Y (2017) Cyclic tests on corrugated steel plate shear walls with openings in modularized-constructions. *Journal of Constructional Steel Research* 138:675-91, DOI: 10.1016/j.jcsr.2017.08.019

Dou C, Jiang ZQ, Pi YL, Guo YL (2016) Elastic shear buckling of sinusoidally corrugated steel plate shear wall. *Engineering Structures* 121:136-146, DOI: 10.1016/j.engstruct.2016.04.047

Edalati SA, Yadollahi Y, Pakar I, Emadi A, Bayat M (2014) Numerical study on the performance of corrugated steel shear walls. *Wind and Structures* 19(4):405-420, DOI: 10.12989/was.2014.19.4.405

Emami F, Mofid M (2014) On the hysteretic behavior of trapezoidally corrugated steel shear walls. *The Structural Design of Tall and Special Buildings* 23(2): 94-104, DOI: 10.1002/tal.1025

Emami F, Mofid M, Vafai A (2013) Experimental study on cyclic behavior of trapezoidally corrugated steel shear walls. *Engineering Structures* 48:750-762, DOI: 10.1016/j.engstruct.2012.11.028

Englekirk R (1994) Steel structures: Controlling behavior through design. John Wiley & Sons Inc, Hoboken, NJ, USA

Esteghamati M, Farzampour A (2020a) Probabilistic seismic assessment of a mid-rise eccentrically braced steel frame equipped with butterfly-shaped dampers. Proceedings of 17th world conference on earthquake engineering, September 13-18, Sandi, Japan

Esteghamati M, Farzampour A (2020b) Probabilistic seismic performance and loss evaluation of a multi-story steel building equipped with butterfly-shaped fuses. *Journal of Constructional Steel Research* 172:106187, DOI: 10.1016/j.jcsr.2020.106187

Esteghamati M, Lee J, Musetich M, Flint M (2020) INSSEPT: An open-source relational database of seismic performance estimation to aid with early design of buildings. *Earthquake Spectra* 36(4):2177-2197, DOI: 10.1177/8755293020919857

Fang J, Bao W, Ren F, Guan T, Xue G, Jiang J (2020) Experimental study of hysteretic behavior of semi-rigid frame with a corrugated plate. *Journal of Constructional Steel Research* 174:106289, DOI: 10.1016/j.jcsr.2020.106289

Farzampour A, Laman JA (2015) Behavior prediction of corrugated steel plate shear walls with openings. *Journal of Constructional Steel Research* 114:258-268, DOI: 10.1016/j.jcsr.2015.07.018

Farzampour A, Mansouri I, Hu JW (2018a) Seismic behavior investigation of the corrugated steel shear walls considering variations of corrugation geometrical characteristics. *International Journal of Steel Structures* 18(4):1297-1305, DOI: 10.1007/s13296-018-0121-z

Farzampour A, Mansouri I, Lee CH, Sim HB, Hu JW (2018b) Analysis and design recommendations for corrugated steel plate shear walls with a reduced beam section. *Thin-Walled Structures* 132(11):658-666, DOI: 10.1016/j.tws.2018.09.026

Farzampour A, Yekrangnia M (2014) On the behavior of corrugated steel shear walls with and without openings. Proceedings of second european conference on earthquake engineering and seismology, August 25-29, Istanbul, Turkey

GB50011-2010 (2010) Code for seismic design of buildings. GB50011-2010, China Architecture and Building Press, Beijing, China (in Chinese)

GB50017-2017 (2017) Standard for design of steel structure. GB50017-2017, China Architecture and Building Press, Beijing, China (in Chinese)

Hamburger R, Rojahn C, Moehle J, Bachman R, Comartin C, Whittaker A (2004) The ATC-58 project: Development of next-generation performance-based earthquake engineering design criteria for buildings. Proceedings of 13th world conference on earthquake engineering, Vancouver, BC, Canada

HAZUS-MH MR5 (2010) Earthquake loss estimation methodology. Technical and User's Manual. Department of Homeland Security, Federal Emergency Management Agency, Mitigation Division, Washington DC, USA

Hosseinzadeh L, Emami F, Mofid M (2017) Experimental investigation on the behavior of corrugated steel shear wall subjected to the different angle of trapezoidal plate. *Structural Design of Tall & Special Buildings* 2017(2):e1390, DOI: 10.1002/tal.1390

Huang YL, Lu XZ, Ye LP, Shi W (2011) A pushover analysis algorithm based on multiple point constraints. *Engineering Mechanics* 28(2): 18-23 (in Chinese)

JGJ99-2015 (2016) Technical specification for steel structure of tall building. JGJ99-2015, China Architecture and Building Press, Beijing, China (in Chinese)

Jiang WW, Jin HJ, Sun FF, Li GQ, Qian P, Tong J, Yan CZ (2019) Research on simplified analysis models of non-buckling corrugated steel shear walls. *Progress in Steel Building Structures* 21(1):61-71

Kalali H, Hajsadeghi M, Zirakian T, Alaee FJ (2015) Hysteretic performance of SPSWs with trapezoidally horizontal corrugated web-plates. *Steel and Composite Structures* 19(2):277-292, DOI: 10.12989/scs.2015.19.2.277

Kharmale SB, Ghosh S (2013) Performance-based plastic design of steel plate shear walls. *Journal of Constructional Steel Research* 90(8):85-97, DOI: 10.1016/j.jcsr.2013.07.029

Lee SS, Goel SC, Chao SH (2004) Performance-based seismic design of steel moment frames using target drift and yield mechanism. Proceedings of 13th world conference on earthquake engineering, Vancouver, BC, Canada

Leelataviwat S (1998) Drift and yield mechanism based seismic design and upgrading of steel moment frames. PhD Thesis, University of Michigan, Ann Arbor, MI, USA

Liu S, Warn GP, Berman JW (2013) Estimating natural periods of steel plate shear wall frames. *Journal of Structural Engineering* 139(1): 155-161, DOI: 10.1061/(ASCE)ST.1943-541X.0000610

Masoud HA, Mahna S (2018) Seismic behavior of steel plate shear wall with reduced boundary beam section. *Thin-Walled Structures* 116: 169-179, DOI: 10.1016/j.tws.2017.03.014

Mitchell D, Tremblay R, Karacabeyli E, Paultre P, Saatcioglu M, Anderson DL (2003) Seismic force modification factors for the proposed 2005 edition of national building code of Canada. *Canadian Journal of Civil Engineering* 30(2):308-327, DOI: 10.1139/l02-111

Newmark NM, Hall WJ (1982) Earthquake spectra and design. Earthquake Engineering Research Institute, Oackland, CA, USA

Paslar N, Farzampour A, Hatami F (2020a) Infill plate interconnection effects on the structural behavior of steel plate shear walls. *Thin-Walled Structures* 149:106621, DOI: 10.1016/j.tws.2020.106621

Paslar N, Farzampour A, Hatami F (2020b) Investigation of the infill plate boundary condition effects on the overall performance of the steel plate shear walls with circular openings. *Structures* 27:824-836, DOI: 10.1016/j.istruc.2020.06.031

Qiu J, Zhao QH, Yu C, Li ZX (2018) Experimental studies on cyclic behavior of corrugated steel plate shear walls. *Journal of Structural Engineering* 144(11):04018200, DOI: 10.1061/(ASCE)ST.1943-541X.0002165

Qu B, Bruneau M (2010) Capacity design of intermediate horizontal boundary elements of steel plate shear walls. *Journal of Structural Engineering* 136(6):665-675, DOI: 10.1061/(ASCE)ST.1943-541X.0000167

Sabelli R, Bruneau M (2007) AISC steel design guide 20: Steel plate shear walls. AISC, Chicago, IL, USA

SEAOC (1995) Vision 2000: Performance-based seismic engineering of buildings. Structural Engineers Association of California, Sacramento, CA, USA

Shariati M, Faegh SS, Mehrabi P, Bahavarnia S, Zandi Y, Masoom D, Toghroli A, Trung N, Salih M (2019) Numerical study on the structural performance of corrugated low yield point steel plate shear walls with circular openings. *Steel and Composite Structures* 33(4):569-581, DOI: 10.12989/scs.2019.33.4.569

SIMULIA (2014) ABAQUS/standard user's manual, version 6.14. Dassault Systèmes Simulia Corp., Providence, RI, USA

Soonsik L (2002) Performance-based design of steel moment frames using target drift and yield mechanism. PhD Thesis, University of Michigan, Ann Arbor, MI, USA

Stojadinovic B, Tipping S (2008) Structural testing of corrugated sheet steel shear walls. Proceedings of 19th international specialty conference on cold-formed steel structures. Missouri University of Science and Technology, Rolla, MO, USA

Sun G, Gu Q, He R, Fang Y (2013) Distribution of horizontal seismic shear based on inelastic state of steel plate shear walls. *Engineering Mechanics* 30(7):113-121, DOI: 10.6052/j.issn.1000-4750.2012.03.0139 (in Chinese)

Topkaya C, Kurban CO (2009) Natural periods of steel plate shear wall systems. *Journal of Constructional Steel Research* 65(3):542-551, DOI: 10.1016/j.jcsr.2008.03.006

Tong JZ, Guo YL (2018) Shear resistance of stiffened steel corrugated shear walls. *Thin-Walled Structures* 127:76-89

Sullivan TJ (2013) Direct displacement-based seismic design of steel eccentrically braced frame structures. *Bulletin of Earthquake Engineering* 11:2197-2231, DOI: 10.1007/s10518-013-9486-8

Yakut A, Yilmaz H (2008) Correlation of deformation demands with ground motion intensity. *Journal of Structural Engineering* 134(12): 1818-1828, DOI: 10.1061/(ASCE)0733-9445(2008)134:12(1818)

Yi J, Gil H, Youm K, Lee H (2008) Interactive shear buckling behavior of trapezoidally corrugated steel webs. *Engineering Structures* 30(6): 1659-1666, DOI: 10.1016/j.engstruct.2007.11.009

Yu Y, Chen Z (2018) Rigidity of corrugated plate sidewalls and its effect on the modular structural design. *Engineering Structures* 175:191-200, DOI: 10.1016/j.engstruct.2018.08.039

Zhang J, Zirakian T (2015) Probabilistic assessment of structures with SPSW systems and LYP steel infill plates using fragility function method. *Engineering Structures* 85(2):195-205, DOI: 10.1016/j.engstruct.2014.12.027

Zhao Y (2018) Lateral behavior and design method of corrugated steel plate shear walls. MSc Thesis, Tianjin University, Tianjin, China (in Chinese)

Zhao Q, Li Y (2016) Buckling and instabilities of sinusoidally corrugated steel plate shear walls. Proceedings of 7th international conference on coupled instabilities in metal structures, November 7-8, 2016, Baltimore, MD, USA

Zhao Q, Qiu J, Zhao Y, Yu C (2020) Estimating fundamental period of corrugated steel plate shear walls. *KSCE Journal of Civil Engineering* 24(10):3023-3033, DOI: 10.1007/s12205-020-2305-2

Zhao Q, Sun JH, Li Y, Li ZX (2017) Cyclic analyses of corrugated steel plate shear walls. *Structural Design of Tall & Special Buildings* 26(16):e1351, DOI: 10.1002/tal.1351